RSC Advances

PAPER

View Article Online
View Journal | View Issue

Cite this: *RSC Adv.*, 2015, **5**, 50883

Intrinsic defects in gallium sulfide monolayer: a first-principles study

Hui Chen, Yan Li,* Le Huang and Jingbo Li*

Received 6th May 2015
Accepted 26th May 2015

DOI: 10.1039/c5ra08329j

www.rsc.org/advances

The electronic and magnetic properties of native point defects, including vacancies (V_{Ga} and V_S), antisites (Ga_S and S_{Ga}) and interstitials (Ga_i and S_i) in monolayer and bulk GaS, were systemically studied using the density functional theory method. For the monolayer, the impurity states appeared in the band gaps of all defect structures except interstitial S_i. Half-metallic behavior can be obtained in the presence of V_{Ga} and Ga_i. Monolayers with V_{Ga}, Ga_S, S_{Ga} and Ga_i had a total magnetic moment of 1.0 μ_B, as did the bulk samples with V_{Ga}, Ga_S and S_{Ga}, whereas the monolayers with V_S and S_i and bulk sample with Ga_i were spin-unpolarized. In addition, n- and p-type GaS monolayers were obtained under Ga-rich and S-rich conditions, respectively. Ga_S and S_{Ga} were identified as suitable n- and p-type defects, respectively.

I. Introduction

Two-dimensional (2D) materials have attracted increasing interest as a result of their exotic transport physics and remarkable electrical, optical, magnetic and mechanical properties.[1–4] The basic photovoltaic and photoelectronic properties of monolayer GaS, a III–VI semiconductor, have been extensively studied in terms of its potential application in solar cells, solid-state batteries and memory devices.[5–13] GaS and GaSe monolayer field-effect transistors have been made with n- and p-type conducting features, respectively.[13] A few-layer GaS two-terminal photodetector with a fast and stable response was fabricated by Yang *et al.*[14] A higher photo-response and external quantum efficiency were obtained in NH_3 than in air or O_2 as a result of the opposite roles that NH_3 and O_2 play during charge transfer between the adsorbed gas molecules and the photodetector. Doped few-layer GaS has also been considered as a promising material for the fabrication of near-blue light-emitting devices by controlling the defects and their electronic properties during preparation.[15]

From the theoretical point of view, the structural and electronic properties of GaS layered compounds have been extensively studied using the density functional theory (DFT) method.[16–23] Zólyomi *et al.*[16] showed that 2D crystals of Ga_2X_2 (X = S, Se and Te) were dynamically stable indirect band gap semiconductors with a sombrero dispersion of holes near the valence band maximum (VBM). Ma *et al.*[17] reported that the band gaps of GaS and GaSe increased from multilayer to single layer structures and could be tuned under mechanical strain, which makes them potential candidates for tunable nanodevices. Orudzhev and Kasumova[18] established that the elastic constants of GaS layered compounds increase monotonically in the pressure range of 0–20 GPa as the pressure increases. Zhou *et al.*[19] demonstrated that GaS nanoribbons can display an intrinsic half-metallic character with ferromagnetic coupling, raising from the Ga-4s, Ga-4p, and S-3p states. Ding and Wang[20] reported characteristic Dirac-like band features in linear dispersions of Si/GaS heterosheets. They also proposed that a sizable band gap at the Dirac point is opened as a result of the intrinsic electronic field and this can be tuned by altering the voltage or strain. Understanding basic information about native and exotic defects is of great importance as structural imperfections, such as lattice defects, may change the electronic, magnetic and optical properties of materials. However, to the best of our knowledge, little work has been reported on the electronic and magnetic properties of native point defects in GaS monolayer.

We investigated the electronic and magnetic properties of intrinsic defects (V_{Ga}, V_S, Ga_S, S_{Ga}, Ga_i and S_i) in GaS monolayer by a first-principles method based on DFT. The formation energies under two different preparation conditions were taken into account: (i) gallium-rich and sulfur-poor conditions; and (ii) gallium-poor and sulfur-rich conditions. We found that, without any doping impurities, GaS monolayer will tend to form an n-type semiconductor under gallium-rich and sulfur-poor conditions, whereas they will tend to form a p-type semiconductor under gallium-poor and sulfur-rich conditions. By analogy, the same results are expected to be applicable to other III–VI semiconductors such as GaSe and GaTe.

II. Computational method

Calculations were performed within DFT using generalized-gradient approximation with the functional of Perdew, Burke

State Key Laboratory for Superlattice and Microstructure, Institute of Semiconductor, Chinese Academy of Science, Beijing 100083, China. E-mail: bclly2008@semi.ac.cn; jbli@semi.ac.cn

and Ernzerhof (PBE) method[24,25] implemented in the Vienna ab initio simulation package.[26,27] For comparison, some calculations were also performed using the Heyd–Scuseria–Ernzerhof (HSE06) hybrid functional.[28,29] The cutoff energy was set to 364 eV. For the GaS monolayer, a unit cell including four atoms was used in the calculations for the pristine GaS monolayer and a large 4×4 supercell with one defect was chosen for the defective monolayer. Brillouin zone sampling was performed with Monkhorst–Pack special k-point meshes.[30] We chose k-point grids of $20 \times 20 \times 1$ and $5 \times 5 \times 1$ to calculate the pristine and defective systems, respectively. The distance between adjacent monolayers was >12 Å and hence the interaction between the monolayers could be eliminated. For bulk GaS, a unit cell containing eight atoms was chosen for the calculations of pristine bulk GaS and a $3 \times 3 \times 1$ supercell including one defect was used for the defect system. $15 \times 15 \times 3$ and $5 \times 5 \times 1$ k-point grids were used in the pristine and defect bulk samples, respectively. The distance between two layers was 7.5 Å. The convergence criteria used for the electronic self-consistent relaxation and the ionic relaxation were set to 10^{-6} eV for energy and 0.02 eV $Å^{-1}$ for force, respectively.

Typical intrinsic defects in the GaS monolayer and bulk sample, including vacancies (V_{Ga} and V_S), antisites (Ga_S and S_{Ga}) and interstitials (Ga_i and S_i) were studied. To search the most stable configuration of the interstitials, four different positions labeled as T_S (at the top of S atoms), T_G (at the top of Ga atoms), C (above the central atom of the hexagonal ring of GaS) and M (above the middle of the Ga–S bond) were considered (Fig. 1).[31]

To determine the formation energy and transition energy levels of a defect, the total energy $E_{D,q}$ of the GaS monolayer containing the defect atom α with charge state q was calculated. The formation energy $\Delta H_{D,q}$ of the defective system was defined as:[32–38]

$$\Delta H_{D,q} = (E_{D,q} - E_H) + \sum_\alpha n_\alpha \mu_\alpha + q(E_V + E_F) \quad (1)$$

where E_H is the total energy of the GaS monolayer without defects,[32,33] n_α is the number of defect atoms ($n_\alpha = -1$ when an atom is added and $n_\alpha = 1$ when an atom is removed), μ_α is the atomic chemical potential[34–36] and q is the number of electrons transferred from the supercell to the reservoirs in the formation of the defective cell.[39] E_V is the energy at the VBM of the defect-free system. Here, the electron Fermi energy E_F is limited between the VBM and the conduction band minimum (CBM). Consequently, the defect formation energy strongly depends on μ_α and E_F.

μ_α can be also expressed as $\mu_\alpha = \mu_\alpha^{solid} + \Delta\mu_\alpha$,[37,40] where μ_α^{solid} is the total energy of solid Ga or S in its stable phase. However, there are some thermodynamic limits on the achievable values of the chemical potentials under thermal equilibrium growth conditions. First, $\Delta\mu_\alpha$ is bound by $\Delta\mu_\alpha \leq 0$ to avoid the precipitation of Ga and S, corresponding to the "α-rich condition". Second, $\Delta\mu_\alpha$ is limited to values that maintain the stable GaS monolayer, through which an "α-poor condition" can be obtained.[39]

The transition level $\varepsilon(D, q/q')$ is the Fermi level position at which the formation energy of defect D at charge state q is equal to that at charge state q', namely, $\Delta H_{D,q} = \Delta H_{D,q'}$.[37,41–43] From eqn (1), the transition energy level can be obtained by:

$$\varepsilon(D,q/q') = [\Delta H_{D,q}(E_F = 0) - \Delta H_{D,q'}(E_F = 0)]/(q' - q) \quad (2)$$

where $\Delta H_{D,q}(E_F = 0)$ is the formation energy of defect D with the charge state q when $E_F = 0$.[41,44] To avoid the problem that using special k-points or equivalent k-points in the superstructure gives a poor description of the symmetry and energy levels of the defect state, a hybrid scheme combining the advantages of both special k-points and Γ-point only approaches was used.[39,45] Core level shifts were also considered.

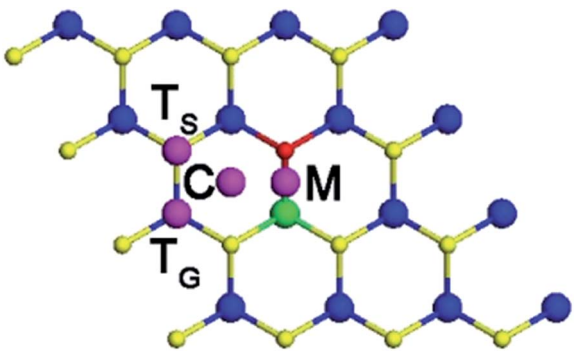

Fig. 1 Schematic structure of the GaS monolayer. The blue, yellow and green (or red) balls represent the Ga, S and intrinsic defect atoms, respectively.

III. Results and discussion

The hexagonal structure of GaS has a layered S–Ga–Ga–S repeating unit built by six-membered Ga_3S_3 rings.[13] The calculated heat of formation was −1.11 eV. The pristine GaS monolayer and bulk sample were both non-magnetic indirect band gap semiconductors. The gap values of the monolayer and bulk sample were 2.58 and 1.60 eV calculated by the PBE method, which were in good agreement with other theoretical results[17] and close to the experimental values of 3.05 (ref. 46) and 2.53 eV,[47] respectively. For comparison, the band gaps of the monolayer and bulk sample were 3.28 and 2.30 eV, respectively, using the HSE06 method. The band structure and density of states of the GaS monolayer and bulk sample calculated by both the PBE and HSE06 methods are plotted in Fig. 2. The VBM and CBM of the GaS monolayer were located near the Γ point and at the M point, respectively, whereas in bulk GaS they were situated at the Γ and M points, respectively. In the GaS monolayer, the lower conduction bands were mainly attributed to the Ga-4s and S-3p states, whereas the lowest conduction bands were attributed to the hybridization of the Ga-4p and S-3p states (Fig. 2b). The uppermost valence bands were primarily from the Ga-4p and S-3p states in addition to a small contribution from the Ga-4s state. The valence bands in the range −3.0 to −1.5 eV were mainly contributed by the Ga-4p and S-3p orbitals, except for a small contribution from the Ga-3d states. The hybridization of the Ga-4p and S-3p orbitals were located at a deeper energy range of about −3.1 eV. The orbital components of the

energy bands in bulk GaS were similar to those of energy bands in the GaS monolayer. By comparing Fig. 2a with c, and b with d, we found that the band structures and density of states of both the GaS monolayer and bulk sample calculated by the PBE method had a similar alignment to the results calculated by the HSE06 method. In view of the huge cost of computing resources and time, the standard PBE functional was considered synthetically in the calculations of the defective systems.

The electronic properties of GaS monolayer with typical native defects were studied. Fig. 3 shows the total density of states and projected density of states of the intrinsic defects in the GaS monolayer. This shows that V_{Ga} and Ga_i doped GaS monolayer are p- and n-type semiconductors, respectively. The impurity states appear in the band gaps of all the defect structures except S_i; the impurity states induced by V_S, Ga_S and S_{Ga} belong to deep-level states in the gaps. Therefore the band gap of the pristine monolayer is evidently tuned, which significantly affects its optical and transport properties. It is clear that the impurity states of V_S are mainly formed by the 4p states of the Ga atom closest to the S vacancy, whereas these impurity states of Ga_S and S_{Ga} are attributed to hybridization between the p states of the substituted atoms and the Ga (S) atom nearest them, with a small contribution from the p states of the nearest S (Ga) atom. It can be seen that V_{Ga} and Ga_i behave as half-metals and can be used as spin filters. Their band structures are shown in Fig. 4. V_{Ga} in sheets behaves as an indirect p-type semiconductor for up-spin channels and as a metal for down-spin channels; the corresponding band gap is 2.18 eV from the M to the Γ point for up-spin electrons. In contrast, for Ga_i, the sheet is metallic for the up-spin channel and an n-type semiconductor with an indirect band gap of 2.47 eV from the k point to the Γ point for the down-spin channel.

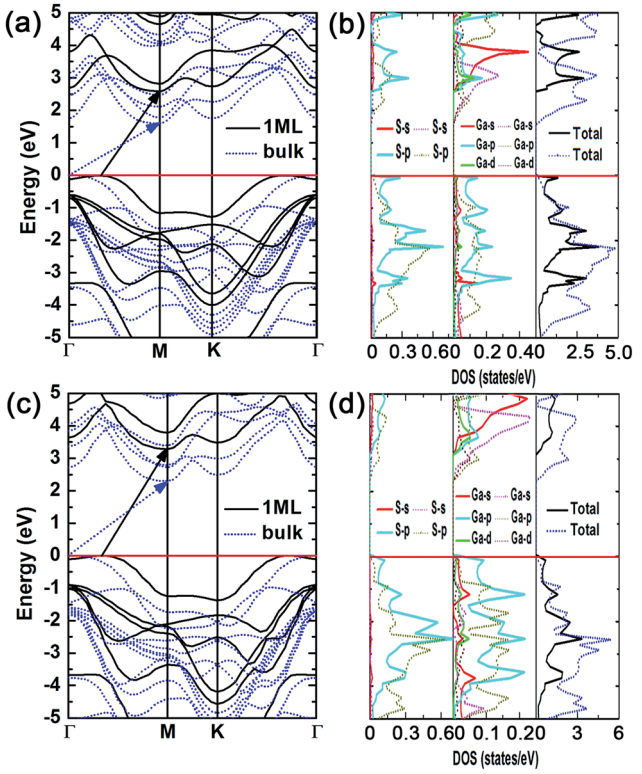

Fig. 2 (a and c) Band structure and (b and d) density of states (DOS) of GaS monolayer compared with the bulk phase using the PBE and HSE06 functionals, respectively. The solid and dotted lines represent the GaS monolayer and bulk phase, respectively. E_F is plotted with respect to the VBM and set to zero.

Bader analysis[48] was used to calculate the charge transfer. For perfect bulk GaS, the loss of electrons on four Ga atoms was 3.05e. For the pristine GaS monolayer, the depletion of electrons on two Ga atoms in total was 1.52e. Table 1 shows that the antisite atoms exchanged smaller amounts of excess electrons with the monolayer compared with other types of defect atoms, especially for substituted Ga atoms in Ga_S; here, 0.114e was subtracted from the Ga substituted atom. The S adatom in S_i exchanged the most excess electrons among all the different types of defect atoms – that is, 0.939e transferred from the monolayer onto the S adatom.

These native defects not only affect the electronic properties, but also bring about magnetic features. To determine the ground state of the GaS monolayer and bulk sample with native defects, we calculated the energy difference between the spin-polarized and spin-unpolarized states (ΔE)[49] (Table 1). V_{Ga}, Ga_S, S_{Ga} and Ga_i in the GaS monolayer had a magnetic ground state, whereas V_S and S_i were spin-unpolarized. All the magnetic moments were 1.0 μ_B per supercell in V_{Ga}, Ga_S, S_{Ga} and Ga_i. However, the contributions of the nearest S atom close to the Ga vacancy in V_{Ga}, the Ga substitution in Ga_S, the S substitution in S_{Ga} and the Ga adatom in Ga_i to the total magnetic moments were unequal at 16.0, 19.4, 12.3 and 9.1%, respectively. Fig. 5 shows that the spin polarization in the monolayer was mainly localized on the dopants and neighboring atoms for the S_{Ga} antisite, whereas larger spatial extensions of spin density were found for the V_{Ga} vacancy, the Ga_S antisite and the Ga_i interstitial. In bulk GaS, V_{Ga}, Ga_S and S_{Ga} had a magnetic ground state with magnetic moments of 1.0 μ_B per supercell, whereas V_S, Ga_i and S_i were spin-unpolarized. The contributions of the nearest S atom close to the Ga vacancy in V_{Ga}, Ga substitution in Ga_S and S substitution in S_{Ga} to the total magnetic moments were 1.0, 20.2 and 5.2%, respectively. The reason for the Ga_i in the monolayer having magnetic properties while it is spin-unpolarized in the bulk sample was thought to be due to the weak Van der Waals forces between adjacent layers.

We now discuss the formation energy of the various native defects in GaS monolayer. The vacancy V_{Ga} is taken as an example to illustrate the relationship between the formation energy and E_F. Fig. 6 shows the formation energies of the acceptor point defect V_{Ga} with the charge state q of 0, 1− and 2−. As the formation energy of V_{Ga} with $q = 2-$ is the lowest among all the charge states, it will be prone to form V_{Ga} ($q = 2-$). As the concentration of cavities increases, E_F will decrease. During the process in which E_F moves downward from the CBM to the VBM, the charge state of V_{Ga} will transfer from 2− to 1− and, finally, to 0. Table 2 lists the calculated formation energies of the intrinsic point defects with each charge state. For the neutral charge state, the formation energy of S_{Ga} is the highest, whereas that of V_S is the lowest under gallium-rich conditions.

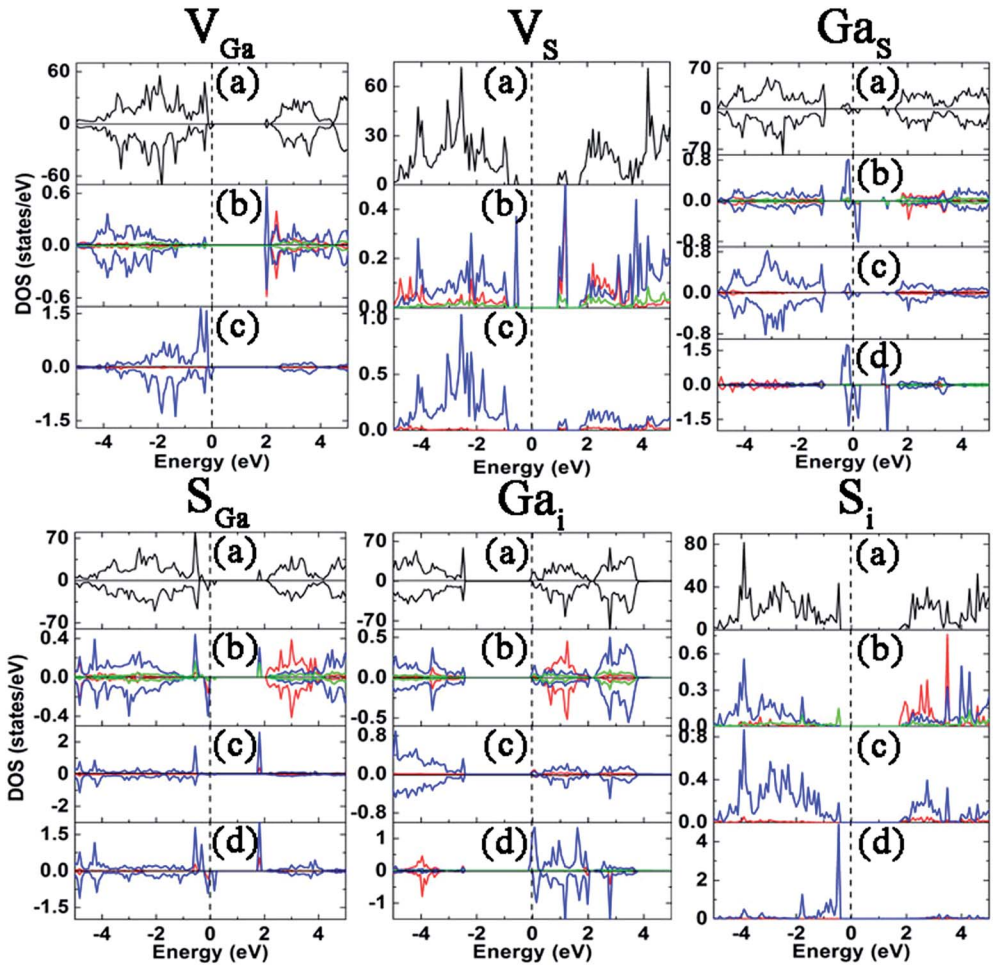

Fig. 3 Total density of states (TDOS) and projected density of states (PDOS) of V_{Ga}, V_S, Ga_S, S_{Ga}, Ga_i and S_i in GaS monolayer. The uppermost plane is TDOS (a). The planes (b), (c) and (d) are the PDOS of the Ga atom, the S atom closest to the defect position and the defect atom, respectively. The red, blue and green lines represent the s, p and d orbitals, respectively. E_F is set to zero.

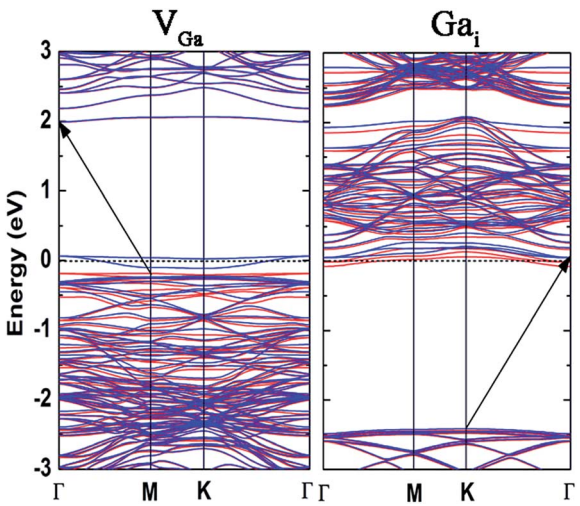

Fig. 4 Band structures of V_{Ga} and Ga_i in GaS monolayer. The red (blue) color corresponds to the up-spin (down-spin) channel. E_F is set to zero.

Therefore GaS will be prone to form V_S donor defect. However, Ga_S has the highest formation energy, whereas S_i has the lowest formation energy under sulfur-rich conditions, which proves that GaS will easily form S_i acceptor defect.

Fig. 7 shows the formation energies of the intrinsic defects in monolayer GaS as a function of E_F under different conditions. Fig. 7a shows the formation energies of the intrinsic defects as a function of E_F under gallium-rich and sulfur-poor conditions. It is clearly seen that the Ga_S defect with $q = 2+$ have the lowest and most negative formation energy near the VBM. Therefore GaS will be prone to form Ga_S donor defect. As the concentration of electrons increases, E_F will move upward. When E_F is located on the crossing point between Ga_S ($q = 2+$) and Ga_i ($q = 1+$), the GaS monolayer will tend to form Ga_i donor defect. Eventually, E_F will stay on the crossing point between Ga_i ($q = 1+$) and S_i ($q = 1-$) and close to the CBM. Therefore GaS will tend to form an n-type semiconductor under gallium-rich conditions.

Fig. 7b shows the formation energies of native defects as a function of E_F under gallium-poor and sulfur-rich conditions. S_{Ga} defect with $q = 3-$ have the lowest and most negative

Table 1 Calculated values for GaS monolayer and bulk sample with native V_{Ga}, V_S, Ga_S, S_{Ga}, Ga_i and S_i defects[a]

Species	Features	V_{Ga}	V_S	Ga_S	S_{Ga}	Ga_i	S_i
Monolayer	$\Delta\rho$	0.645	−0.496	−0.114	0.337	−0.543	0.939
	ΔE	−0.059	—	−0.057	−0.099	−0.001	—
	μ_{total}	1.00	—	1.00	1.00	1.00	—
	μ	0.19	—	0.24	0.14	0.10	—
Bulk	$\Delta\rho$	0.733	−0.490	−0.138	0.351	−0.685	0.296
	ΔE	−0.002	—	−0.005	−0.006	—	—
	μ_{total}	1.00	—	1.00	1.00	—	—
	μ	0.01	—	0.253	0.055	—	—

[a] $\Delta\rho$ (e), excess charge on dopant or the nearest atom close to the vacancy; ΔE (eV), energy difference between magnetic and non-magnetic states; μ_{total} (μ_B), magnetic moments of the whole supercell and dopant or the nearest atom close to the vacancy μ (μ_B).

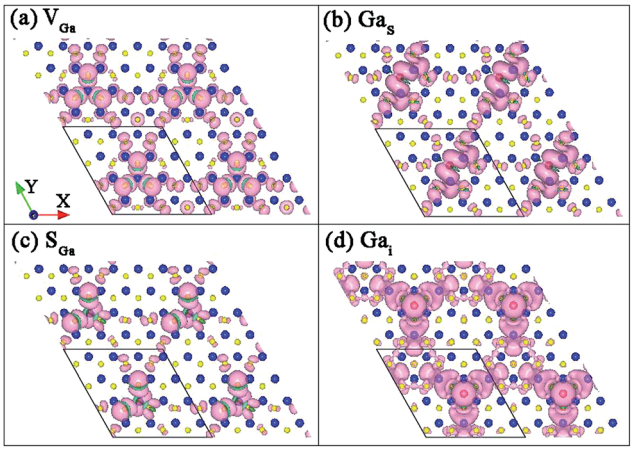

Fig. 5 Spin density isosurfaces of GaS monolayer with native defects: (a) V_{Ga}; (b) Ga_S; (c) S_{Ga}; and (d) Ga_i. The isosurface value is set to 0.0002e Å^{-3}. The pink and green colors represent positive and negative values, respectively.

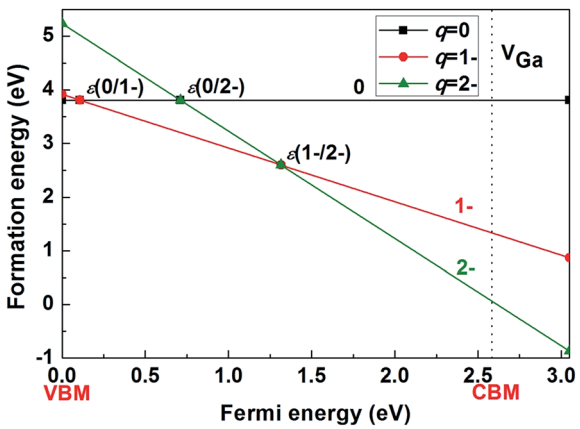

Fig. 6 Calculated formation energy of vacancy V_{Ga} in GaS as a function of E_F under Ga-rich and S-poor conditions ($\Delta\mu_{Ga} = 0$ and $\Delta\mu_S = -1.114$ eV). The zero point of E_F corresponds to the VBM. The dotted line corresponds to the CBM in the calculation.

formation energies among all the intrinsic defects near the CBM. Consequently, GaS will tend to form S_{Ga} acceptor defects. As the concentration of cavity carriers increases, E_F will remove

Table 2 Calculated defect formation energies ΔH at $E_F = 0$ for intrinsic defects in GaS monolayer under Ga-rich ($\Delta\mu_{Ga} = 0$ and $\Delta\mu_S = -1.114$ eV) and S-rich conditions ($\Delta\mu_S = 0$ and $\Delta\mu_{Ga} = -1.114$ eV)

		ΔH (eV)	
Defects	q	Ga-rich	S-rich
Ga_i	1+	−0.980	0.134
	0	1.618	2.733
Ga_S	2+	−2.359	−0.131
	1+	−0.373	1.855
	0	1.912	4.140
V_S	2+	−1.499	−0.385
	1+	−0.246	0.868
	0	0.948	2.063
V_{Ga}	0	3.811	2.697
	1−	3.918	2.804
	2−	5.234	4.120
S_i	0	2.073	0.959
	1−	2.467	1.353
S_{Ga}	0	5.034	2.805
	1−	6.067	3.839
	2−	6.860	4.631
	3−	8.126	5.897

downward. When E_F is located on the crossing point between S_i ($q = 1-$) and S_{Ga} ($q = 3-$), the GaS monolayer will be prone to form S_i acceptor defects. Eventually, E_F will remain on the crossing point between Ga_i ($q = 1+$) and S_i ($q = 1-$) and close to the VBM. Therefore GaS tends to form a p-type semiconductor under sulfur-rich conditions.

Table 3 lists the transition levels $\varepsilon(q/q')$ of each point defect with respect to the VBM. To obtain n-type semiconductors, the primary donor defect should have a high transition level and low formation energy. Table 3 shows that the donor defect Ga_i has the highest transition level $\varepsilon(1+/0)$ and is closest to the CBM. Thus Ga_i can provide abundant electron carriers to form n-type GaS monolayer. However, the formation energy of the donor defect Ga_S is lower than that of Ga_i in any case when E_F is close to the VBM; therefore GaS monolayer does not tend to form Ga_i donor defect (Fig. 7a). Although Ga_S defect has a transition energy $\varepsilon(1+/0)$ lower only than that of Ga_i, in view of the fact that GaS tends to form Ga_S defect more easily, Ga_S becomes the

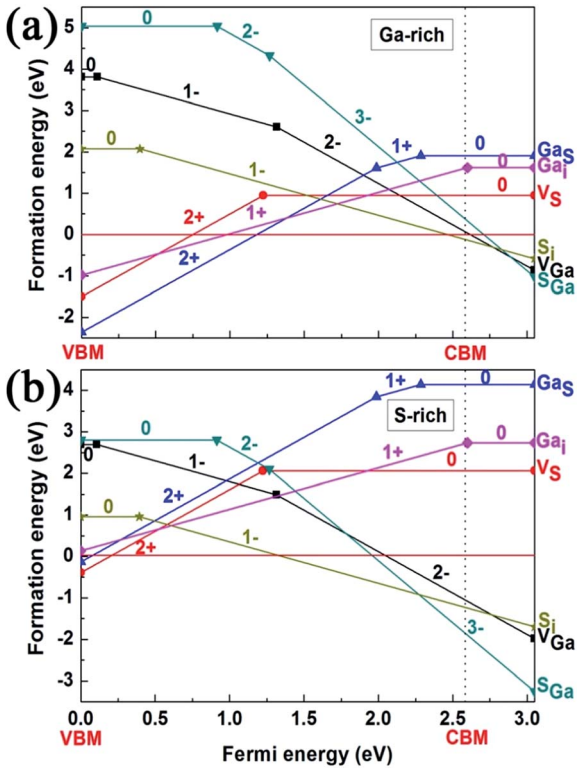

Fig. 7 Formation energies of intrinsic defects in GaS monolayer as a function of E_F under (a) Ga-rich and S-poor conditions ($\Delta\mu_{Ga} = 0$ and $\Delta\mu_S = -1.114$ eV) and (b) Ga-poor and S-rich conditions ($\Delta\mu_S = 0$ and $\Delta\mu_{Ga} = -1.114$ eV). The zero point of E_F corresponds to the VBM and the formation energies have been plotted up to the CBM with the experimental band gap (3.05 eV). The red horizontal line corresponds to a formation energy of zero. The slope of the line represents the charge state q labeled above each line.

primary defect in n-type GaS despite its lower transition energy relative to Ga_i. We deduced that, to obtain an n-type semiconductor, the GaS monolayer should be prepared under gallium-rich conditions. On the other hand, to obtain p-type semiconductors, the dominant acceptor defect should have a low transition level and low formation energy. Table 3 shows that the acceptor defect V_{Ga} with the lowest transition energy level $\varepsilon(0/1-)$ is closest to the VBM. This indicates that the V_{Ga} defect can provide p-type GaS with sufficient concentrations of

Table 3 Calculated transition energy levels $\varepsilon(q/q')$ of intrinsic defects in GaS monolayer with respect to the VBM

Defects	q/q'	$\varepsilon(q/q')$ (eV)
Ga_i	1+/0	2.598
Ga_S	2+/1+	1.986
	1+/0	2.285
V_S	2+/0	1.224
V_{Ga}	0/1−	0.107
	1−/2−	1.316
S_i	0/1−	0.394
S_{Ga}	0/2−	0.913
	2−/3−	1.266

cavities. However, the formation energy of the acceptor defect S_{Ga} is lowest among all the acceptor defects in any case when E_F is close to the CBM; accordingly, the GaS monolayer does not tend to form V_{Ga} acceptor defect (Fig. 7b). Although the S_{Ga} defect has a transition energy $\varepsilon(0/2-)$ higher than that of V_{Ga}, because GaS tends to form S_{Ga} defect more easily, S_{Ga} is the primary defect in p-type GaS despite its higher transition energy relative to V_{Ga}. From this discussion, we can predict that, to achieve a p-type GaS monolayer, preparation should take place under sulfur-rich conditions.

IV. Conclusions

We have studied the electronic and magnetic properties of the intrinsic point defects V_{Ga}, V_S, Ga_S, S_{Ga}, Ga_i and S_i in GaS monolayer and bulk sample on the basis of first-principles calculations. We also investigated the formation energies and transition energy levels of these defects in the monolayer. In the GaS monolayer, the impurity states exist in the band gaps of all the defects except the interstitial S_i. Furthermore, half-metallic behavior can be attained in the presence of V_{Ga} and Ga_i. Although monolayers with V_{Ga}, Ga_S, S_{Ga} and Ga_i defects and bulk samples with V_{Ga}, Ga_S and S_{Ga} defects gain a total magnetic moment of 1.0 μ_B, monolayers with V_S and S_i and bulk sample with Ga_i defect are spin-unpolarized. Monolayer GaS will tend to form an n-type semiconductor under gallium-rich condition, but will tend to form a p-type semiconductor under sulfur-rich condition. Among the possible intrinsic defects, Ga_S and S_{Ga} are considered to be appropriate n- and p-type defects, respectively. These results provide an effective way to regulate the structural and electronic properties of GaS monolayer.

Author contributions

H.C. performed the density functional theory calculations. H.C., Y.L. and L.H. wrote the manuscript. J.L. guided the work. All authors have read the manuscript.

Acknowledgements

This work was supported by the National Science Foundation of China under Grant no. 91233120 and the National Basic Research Program of China (2011CB921901).

Notes and references

1 A. K. Geim and K. S. Novoselov, *Nat. Mater.*, 2007, **6**, 183.
2 A. K. Geim, *Science*, 2009, **324**, 1530.
3 C. N. R. Rao, A. K. Sood, K. S. Subrahmanyam and A. Govindaraj, *Angew. Chem., Int. Ed.*, 2009, **48**, 7752.
4 C. N. R. Rao, A. K. Sood, R. Voggu and K. S. Subrahmanyam, *J. Phys. Chem. Lett.*, 2010, **1**, 572.
5 A. Kuhn, A. Bourdon, J. Rigoult and A. Rimsky, *Phys. Rev. B: Condens. Matter Mater. Phys.*, 1982, **25**, 4081.
6 M. Gatulle, M. Fischer and A. Chevy, *Phys. Status Solidi B*, 1983, **119**, 327.
7 M. Gatulle and M. Fischer, *Phys. Status Solidi B*, 1984, **121**, 59.

8 R. S. Madatov, A. I. Najafov, T. B. Tagiev and A. R. Mobili, *Inorg. Mater.*, 2008, **44**, 100.
9 G. Shen, D. Chen, P.-C. Chen and C. Zhou, *ACS Nano*, 2009, **3**, 1115.
10 G. Sinha, S. K. Panda, A. Datta, P. G. Chavan, D. R. Shinde, M. A. More, D. S. Joag and A. Patra, *ACS Appl. Mater. Interfaces*, 2011, **3**, 2130.
11 Q. S. Xin, S. Conrad and X. Y. Zhu, *Appl. Phys. Lett.*, 1996, **69**, 1244.
12 F. J. Manjón, A. Segura and V. Muñoz, *J. Appl. Phys.*, 1997, **81**, 6651.
13 D. J. Late, B. Liu, J. Luo, A. Yan, H. S. S. R. Matte, M. Grayson, C. N. R. Rao and V. P. Dravid, *Adv. Mater.*, 2012, **24**, 3549.
14 S. Yang, Y. Li, X. Wang, N. Huo, J.-B. Xia, S.-S. Li and J. Li, *Nanoscale*, 2014, **6**, 2582.
15 D. J. Late, B. Liu, H. S. S. R. Matte, C. N. R. Rao and V. P. Dravid, *Adv. Funct. Mater.*, 2012, **22**, 1894.
16 V. Zólyomi, N. D. Drummond and V. I. Fal'ko, *Phys. Rev. B: Condens. Matter Mater. Phys.*, 2013, **87**, 195403.
17 Y. Ma, Y. Dai, M. Guo, L. Yu and B. Huang, *Phys. Chem. Chem. Phys.*, 2013, **15**, 7098.
18 G. S. Orudzhev and E. K. Kasumova, *Phys. Solid State*, 2014, **56**, 619.
19 Y. Zhou, S. Li, W. Zhou, X. Zu and F. Gao, *Sci. Rep.*, 2014, **4**, 5773.
20 Y. Ding and Y. Wang, *Appl. Phys. Lett.*, 2013, **103**, 043114.
21 B. Wen, R. Melnik, S. Yao and T. Li, *Mater. Sci. Semicond. Process.*, 2010, **13**, 295.
22 Z. Zhu, Y. Cheng and U. Schwingenschlögl, *Phys. Rev. Lett.*, 2012, **108**, 266805.
23 L. Huang, Z. Chen and J. Li, *RSC Adv.*, 2015, **5**, 5788.
24 J. P. Perdew, K. Burke and M. Ernzerhof, *Phys. Rev. Lett.*, 1996, **77**, 3865.
25 P. E. Blöchl, *Phys. Rev. B: Condens. Matter Mater. Phys.*, 1994, **50**, 17953.
26 G. Kresse and J. Hafner, *Phys. Rev. B: Condens. Matter Mater. Phys.*, 1993, **47**, 558.
27 G. Kresse and J. Furthmüller, *Phys. Rev. B: Condens. Matter Mater. Phys.*, 1996, **54**, 11169.
28 J. Heyd and G. E. Scuseria, *J. Chem. Phys.*, 2003, **118**, 8207.
29 J. Heyd, G. E. Scuseria and M. Ernzerhof, *J. Chem. Phys.*, 2006, **124**, 219906.
30 H. J. Monkhorst and J. D. Pack, *Phys. Rev. B: Condens. Matter Mater. Phys.*, 1976, **13**, 5188.
31 S. B. Zhang and S.-H. Wei, *Appl. Phys. Lett.*, 2002, **80**, 1376.
32 S. B. Zhang and J. E. Northhrup, *Phys. Rev. Lett.*, 1991, **67**, 2339.
33 G. A. Baraff and M. Schlüter, *Phys. Rev. Lett.*, 1985, **55**, 1327.
34 S. B. Zhang and J. E. Northrup, *Phys. Rev. Lett.*, 1991, **67**, 2339.
35 D. B. Laks, C. G. Van de Walle, G. F. Neumark, P. E. Blöchl and S. T. Pantelides, *Phys. Rev. B: Condens. Matter Mater. Phys.*, 1992, **45**, 10965.
36 C. Persson, Y.-J. Zhao, S. Lany and A. Zunger, *Phys. Rev. B: Condens. Matter Mater. Phys.*, 2005, **72**, 035211.
37 H. Chen, C.-Y. Wang, J.-T. Wang, X.-P. Hu and S.-X. Zhou, *J. Appl. Phys.*, 2012, **112**, 084513.
38 J. He, K. Wu, R. Sa, Q. Li and Y. Wei, *Appl. Phys. Lett.*, 2010, **96**, 082504.
39 S.-H. Wei, *Comput. Mater. Sci.*, 2004, **30**, 337.
40 J. Pohl and K. Albe, *J. Appl. Phys.*, 2010, **108**, 023509.
41 S.-H. Wei and S. B. Zhang, *Phys. Rev. B: Condens. Matter Mater. Phys.*, 2002, **66**, 155211.
42 A. Janotti and C. G. Van de Walle, *Phys. Rev. B: Condens. Matter Mater. Phys.*, 2007, **76**, 165202.
43 A. Alkauskas, P. Broqvist and A. Pasquarello, *Phys. Status Solidi B*, 2011, **248**, 775.
44 H. Chen, C.-Y. Wang, J.-T. Wang, Y. Wu and S.-X. Zhou, *Phys. B*, 2013, **413**, 116.
45 Y. Yan and S.-H. Wei, *Phys. Status Solidi B*, 2008, **245**, 641.
46 P. Hu, L. Wang, M. Yoon, J. Zhang, W. Feng, X. Wang, Z. Wen, J. C. Idrobo, Y. Miyamoto, D. B. Geohegan and K. Xiao, *Nano Lett.*, 2013, **13**, 1649.
47 C. H. Ho and S. L. Lin, *J. Appl. Phys.*, 2006, **100**, 083508.
48 G. Henkelman, A. Arnaldsson and H. Jónsson, *Comput. Mater. Sci.*, 2006, **36**, 354.
49 Q. Yue, S. Chang, S. Qin and J. Li, *Phys. Lett. A*, 2013, **377**, 1362.